An expansion based on System Equivalent Model Mixing: from a limited number of points to a full-field dynamic response

Miha Kodrič[a], Tomaž Bregar[b], Gregor Čepon[a,*], Miha Boltežar[a]

[a] *University of Ljubljana, Faculty of Mechanical Engineering, Aškerčeva 6, 1000 Ljubljana, Slovenia*
[b] *Gorenje d.o.o., Partizanska 12, 3503 Velenje, Slovenia*

Cite as:
Miha Kodričar, Tomaž Bregar, Gregor Čepon, Miha Boltežar,
An expansion based on System Equivalent Model Mixing: from a limited number of points to a full-field dynamic response, Measurement, 2022, https://doi.org/10.1016/j.measurement.2021.110522

Abstract

A high-resolution dynamic response is important for characterizing a system's dynamic properties. Measurements involving a limited number of points on the structure can be expanded to unmeasured points through approximation or model-based expansion techniques that rely on the introduction of a numerical model. Recently, an expansion method called System Equivalent Model Mixing (SEMM) was proposed where a numerical DoF set is used to extend an experimental model with limited measurement points. The concept of SEMM is similar to the well-known SEREP and VIKING expansion methods, but it is defined in the frequency domain. Using the dynamic substructuring approach, the equivalent experimental and numerical models are coupled so that the hybrid model inherits the dynamic properties of both models. Although the method has been well adopted, there is still no comprehensive phenomenological analysis to determine the influence of the method's parameters on the consistency of the hybrid model and thus on the accuracy of the expansion process. This paper addresses the issue by evaluating the accuracy of the SEMM expansion process, focusing on the influence of the regularity of the so-called equivalent numerical model. The introduction of quasi-equivalent numerical models into SEMM is analysed here, which can differ not only with respect to the mass and stiffness properties but also in terms of the geometry and boundary conditions. The parametric study was carried out on a real component of a household appliance, and the most influential parameters in terms of accuracy of the SEMM expansion process were identified. The analysis showed that accurate expansion results, with a small number of experimental points, is achieved if only those points are well scattered across the analysed system.

Keywords: Experimental model, Full-field response, Expansion process, System equivalent model mixing, Dynamic substructuring, Frequency domain

1. Introduction

A dynamic response measurement is important for the design and optimization of the vibro-acoustic properties of a complex system. Experimental modelling is crucial structural dynamics analysis, as it contains properties that are analytically difficult to obtain [1]. The conventional measurement methods using accelerometers or laser vibrometers allow the user to acquire the dynamic information only at a discrete point. The weakness of this approach is that the measurements are usually carried out on a limited number of points, due to the time-consuming experimental testing, difficult accessibility or limited amount of measuring equipment [2].

More advanced experimental techniques to acquire dense system response involve laser scanning vibrometer [3, 4, 5] and optical methods such as Digital Image Correlation and Digital Photogramme-

*Corresponding author
Email address: gregor.cepon@fs.uni-lj.si (Gregor Čepon)

try [6, 7], enabling full-field, non-contact vibration measurements. To obtain a 3D structural response, several measurement systems must be arranged in an appropriate configuration (e.g., stereo) to reconstruct the spatial displacement response. This proves to be a tedious task that requires an advanced and expensive experimental setup, often combined with a demanding post-processing procedure. In addition, this type of experimental setup enables only a line-of-sight measurement, thus responses of hidden components are inaccessible [8].

Alternatives to determining the dynamic properties in unmeasured degrees of freedom (DoFs) are the model-updating and expansion methods. Model updating is an iterative procedure of updating the numerical model in such a way that it converges with the measurement results [9, 10]. Many model-updating techniques have been proposed, tested and published. They can be subdivided according to the type of measured data used and the model parameters that are updated [11]. All these methods are usually very time-consuming and involve computationally intensive operations.

On the other hand, expansion methods enable the expansion of the measurement at a limited number of points to a denser set of DoFs. The majority of techniques rely on finite-element (FE) numerical models, which present a framework for the expansion process, and are therefore classified as model-based methods [12]. Chen et al. [8] proposed a non-model-based expansion technique, where the measurements at a limited number of points are expanded to a full-field dynamic response without the need for a FE model. The method is defined in the modal space and uses orthogonal primary functions called shape functions to expand the experimental mode shapes. This polynomial-based expansion technique has been used for the dynamic characterization of plate-like structures [8] and also for cylindrical shell structures [13].

More established model-based expansion methods rely on a FE-based transformation matrix, mapping the limited measured DoFs to the augmented set of DoFs [14]. There are several well-established expansion techniques developed in the modal space. The System Equivalent Reduction-Expansion Process (SEREP) was proposed in [15] and has commonly been used for the expansion of data at limited points in a variety of applications [16, 17, 18]. To extend the applicability of the SEREP procedure, a set of data-conditioning techniques known as the Variability Improvement of Key Inaccurate Node Groups (VIKING) [19]) are applied. An advantage of the modal methods is the ability to select fewer target modes than measured DoFs and thereby induce a smoothing of the results.

Since the measured data are usually in the form of frequency-response functions (FRFs), Klassen et al. [20] introduced the System Equivalent Model Mixing (SEMM) method, which can be considered as an expansion method, fully defined in the frequency domain. With the use of SEMM, equivalent models of the same structure are dynamically coupled using the Dynamic Substructuring approach [21]. Theoretically, a numerical and experimental model can be coupled to form a new hybrid model that consists of experimental dynamic properties and contains the DoF set provided by a numerical model. The SEMM method does not rely on modal identification, which can be problematic when it comes to real systems that exhibit a high modal density [22, 23], strong damping [24] and near-to-node sensor positioning [25].

The SEMM method is already an established expansion method, and is used in a variety of applications, such as joint identification [26], correction of noisy data from high-speed cameras [27], data-consistency identification [28, 29], admittance estimation from acoustics measurements [30] and applications in the automotive industry [31].

Although the SEMM method has been widely adopted, there is still no general study to identify the influential parameters and their effect on the accuracy of the expansion process [32]. This paper addresses the issue by evaluating the accuracy of the SEMM expansion process, especially in terms of the regularity of the so-called equivalent numerical model. In fact, the article introduces a quasi-equivalent numerical model to the SEMM method and analyses the effect of boundary conditions, geometry simplification and material properties on the consistency of the expansion process. In addition, the variation of the experimental model is also analysed with respect to the number and distribution of the excitation and response points.

The parametric study is performed on a real-life component of a household appliance to identify the most influential parameters of the SEMM expansion process. The analysis was performed with five different numerical models, which differs in terms of geometry and boundary conditions. The quality

of the expansion process was accessed using the FRAC and MAC criteria, comparing the expanded full-field vibration response with the actual reference measured response.

The results show that the expansion process is more accurate the more excitation and response points are included in the experimental model. An accurate expansion process with a small number of response and excitation points is feasible only when the experimentally observed DoFs are well scattered over the given object and the numerical model presents consistent basics for the expansion process. Based on the presented analysis, guidelines are given for the proper selection of the parameters in the SEMM expansion process.

The paper is organized as follows. The following section briefly summarizes the theory of the SEMM method. Next, the full-field expansion using the SEMM method to mix quasi-equivalent models is presented in Section 3. In Section 4, systematic analyses of the proposed method are performed on a complex structure presented by the side panel of the washing machine. Finally, the conclusions are drawn in Section 5.

2. System equivalent model mixing (SEMM)

The SEMM method was introduced by Klassen et al. [20] and is based on the dynamic substructuring approach using Lagrange multiplier frequency-based substructuring (LM FBS) [21]. While the LM FBS method tries to couple the response models of multiple different structures, the SEMM method assembles equivalent models on a single substructure. For the sake of completeness, a basic recap of the LM FBS method theory is presented [33]. To consider n subsystems, all the local matrices are incorporated into a block-diagonal form. The equation of motion of the discrete dynamic subsystem in the frequency domain is:[1]

$$\boldsymbol{u} = \mathbf{Y}\left(\boldsymbol{f} + \boldsymbol{g}\right), \text{ where: } \mathbf{Y} = \begin{bmatrix} \mathbf{Y}^1 & & \\ & \ddots & \\ & & \mathbf{Y}^n \end{bmatrix}, \ \boldsymbol{u} = \begin{bmatrix} \boldsymbol{u}^1 \\ \vdots \\ \boldsymbol{u}^n \end{bmatrix}, \ \boldsymbol{f} = \begin{bmatrix} \boldsymbol{f}^1 \\ \vdots \\ \boldsymbol{f}^n \end{bmatrix}, \ \boldsymbol{g} = \begin{bmatrix} \boldsymbol{g}^1 \\ \vdots \\ \boldsymbol{g}^n \end{bmatrix}. \tag{1}$$

The vector of DoFs is $\boldsymbol{u}$ and represents the responses to the external force vector $\boldsymbol{f}$ and $\boldsymbol{g}$ is the vector of connecting forces with the other substructures to assure equilibrium conditions. The admittance matrix of all the considered subsystems in block-diagonal form is denoted with $\mathbf{Y}$. The compatibility and equilibrium conditions are introduced with the signed Boolean matrix $\mathbf{B}$ (Eq. (2)), where the interface forces are represented by the Lagrange multipliers vector $\boldsymbol{\lambda}$.

$$\mathbf{B}\,\boldsymbol{u} = \mathbf{0}, \quad \boldsymbol{g} = -\mathbf{B}^{\mathrm{T}}\boldsymbol{\lambda} \tag{2}$$

Using the equilibrium and compatibility conditions and eliminating the Lagrange multiplier vector $\boldsymbol{\lambda}$, the coupled structure's response is obtained, presenting the basic equation for the whole SEMM theory:

$$\boldsymbol{u} = \tilde{\mathbf{Y}}\,\boldsymbol{f} = \left[\mathbf{Y} - \mathbf{Y}\,\mathbf{B}^{\mathrm{T}}\left(\mathbf{B}\,\mathbf{Y}\,\mathbf{B}^{\mathrm{T}}\right)^{-1}\mathbf{B}\,\mathbf{Y}\right]\boldsymbol{f}. \tag{3}$$

The SEMM method is based on the parent model (Fig. 1a), providing the DoF set. The overlay model (Fig. 1b) introduces the real dynamic properties. To form the final hybrid model (Fig. 1d), the dynamic properties of the parent model are eliminated with the removed model (Fig. 1c).

The procedure applies a substructuring approach to expand the model dynamics contained in an overlay model $\mathbf{Y}_{\mathrm{ov}}$ onto the DoF space of a parent model $\mathbf{Y}_{\mathrm{par}}$ [34]. Following Eq. (1) the response of the hybrid model can be formulated as:

$$\boldsymbol{u} = \mathbf{Y}\left(\boldsymbol{f} + \boldsymbol{g}\right), \text{ where: } \mathbf{Y} = \begin{bmatrix} \mathbf{Y}^{\mathrm{par}} & & \\ & -\mathbf{Y}^{\mathrm{rem}} & \\ & & \mathbf{Y}^{\mathrm{ov}} \end{bmatrix}, \ \boldsymbol{u} = \begin{bmatrix} \boldsymbol{u}^{\mathrm{par}} \\ \boldsymbol{u}^{\mathrm{rem}} \\ \boldsymbol{u}^{\mathrm{ov}} \end{bmatrix}, \ \boldsymbol{f} = \begin{bmatrix} \boldsymbol{f}^{\mathrm{par}} \\ \boldsymbol{f}^{\mathrm{rem}} \\ \boldsymbol{f}^{\mathrm{ov}} \end{bmatrix}, \ \boldsymbol{g} = \begin{bmatrix} \boldsymbol{g}^{\mathrm{par}} \\ \boldsymbol{g}^{\mathrm{rem}} \\ \boldsymbol{g}^{\mathrm{ov}} \end{bmatrix}. \tag{4}$$

[1] An explicit dependency on frequency is omitted to improve the readability of the notation, as will be the case for the remainder of the paper.

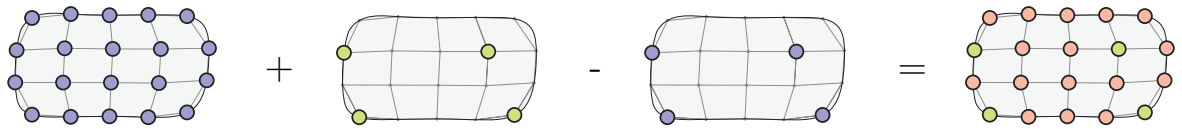

(a) (b) (c) (d)

Figure 1: Equivalent models for SEMM method; a) Parent model $\mathbf{Y}^{\mathrm{par}}$, b) Overlay model $\mathbf{Y}^{\mathrm{ov}}$, c) Removed model $\mathbf{Y}^{\mathrm{rem}}$, d) Hybrid model $\mathbf{Y}^{\mathrm{SEMM}}$.

The DoF set of the parent model contains the internal (i) and boundary (b) DoFs. The boundary DoFs must overlap with the overlay model so the dynamic coupling can be performed, while the internal DoFs of the parent model can be unique. The equivalent models appearing in the SEMM method are arranged by separating the internal and boundary DoFs in the admittance matrices:

$$\mathbf{Y}^{\mathrm{par}} = \begin{bmatrix} \mathbf{Y}_{\mathrm{ii}} & \mathbf{Y}_{\mathrm{ib}} \\ \mathbf{Y}_{\mathrm{bi}} & \mathbf{Y}_{\mathrm{bb}} \end{bmatrix}^{\mathrm{par}}, \quad \mathbf{Y}^{\mathrm{ov}} = [\mathbf{Y}_{\mathrm{bb}}]^{\mathrm{ov}}, \quad \mathbf{Y}^{\mathrm{rem}} = [\mathbf{Y}_{\mathrm{bb}}]^{\mathrm{par}}. \tag{5}$$

The process of dynamic decoupling of the removed model and the coupling of the overlay model to the parent model are achieved by applying compatibility and equilibrium conditions between all the models, just like for coupling the multiple subsystems (Eq. (2)). Following the LM FBS methodology by elimination of the Lagrange multiplier, the final equation is defined as:

$$\overline{\mathbf{Y}} = \mathbf{Y} - \mathbf{Y}\,\mathbf{B}^{\mathrm{T}} \left(\mathbf{B}\,\mathbf{Y}\,\mathbf{B}^{\mathrm{T}}\right)^{-1} \mathbf{B}\,\mathbf{Y}. \tag{6}$$

By considering the localization matrix, a reformulation to primal notation is achieved and the single-line form of the basic SEMM method using primary admittance can be written as:

$$\mathbf{Y}^{\mathrm{SEMM}} = [\mathbf{Y}]^{\mathrm{par}} - \begin{bmatrix} \mathbf{Y}_{\mathrm{ib}} \\ \mathbf{Y}_{\mathrm{bb}} \end{bmatrix}^{\mathrm{par}} (\mathbf{Y}^{\mathrm{rem}})^{-1} (\mathbf{Y}^{\mathrm{rem}} - \mathbf{Y}^{\mathrm{ov}}) (\mathbf{Y}^{\mathrm{rem}})^{-1} [\mathbf{Y}_{\mathrm{bi}}\,\mathbf{Y}_{\mathrm{bb}}]^{\mathrm{par}}. \tag{7}$$

The basic SEMM method also has some extensions increasing its robustness [20]. One of them is the ability to remove spurious peaks, which are a consequence of the conflicting dynamics between the models [34]. If the removed interface is extended to all the internal DoFs ($\mathbf{Y}^{\mathrm{par}} = \mathbf{Y}^{\mathrm{rem}}$), then the final form of the fully extended SEMM method in a single-line[2] notation is:

$$\mathbf{Y}^{\mathrm{SEMM}} = \mathbf{Y}^{\mathrm{par}} - \mathbf{Y}^{\mathrm{par}} ([\mathbf{Y}_{\mathrm{bi}}\,\mathbf{Y}_{\mathrm{bb}}]^{\mathrm{rem}})^{+} (\mathbf{Y}_{\mathrm{bb}}^{\mathrm{rem}} - \mathbf{Y}^{\mathrm{ov}}) \left(\begin{bmatrix} \mathbf{Y}_{\mathrm{ib}} \\ \mathbf{Y}_{\mathrm{bb}} \end{bmatrix}^{\mathrm{rem}} \right)^{+} \mathbf{Y}^{\mathrm{par}}. \tag{8}$$

3. Using SEMM as an expansion technique

Here, the procedure for expanding the measurements from a limited number of points to a full-field dynamic response using the SEMM method is presented. Conventionally, the SEMM method is intended for coupling equivalent models of the same structure, whereby the numerical model is considered as a digital twin of the experimental model [20].

We are often interested in the detailed dynamic response of only a certain sub-component in the system. In that case, numerical modelling of the entire system and its experimental validation proves to be very tedious [35] or, in some cases, even an impossible task [36]. Therefore, it would be convenient if we could obtain the vibrational response of the specific sub-component, by measuring its response at the limited number of points and then obtain a full-field response by expansion using the SEMM method.

The SEMM method performs the expansion by dynamic coupling of the experimental model with a numerical model that introduces consistency between given DoFs. Therefore, the numerical model must

[2] A complete derivation of a single-line formulation is here omitted due to the clarity of the article; an interested reader is referred to [20].

provide proper physical connections between the DoFs. It is well known that the SEMM expansion gives reliable results in the case of an accurate numerical model [37].

Here we propose a different methodology for the SEMM formulation. The experimental model is acquired on a real sub-component, mounted in the assembled configuration, while the numerical model represents the analysed structure decoupled from the rest of the system.

The whole idea is shown schematically in Fig. 2. It is proposed that a sub-component's numerical model is developed independently of the rest of the system. However, the question arises as to how accurate the numerical model must be to consider it as equivalent to the experimental model. The accuracy of the numerical model is strongly influenced by the applied boundary conditions. These are difficult to model, taking into account the connections with other sub-components in the entire system. In addition, in some cases, the detailed geometries of the components are not even accessible, as in the case with complex electromechanical components.

The article systematically analyses the possibility of including a so-called quasi-equivalent numerical model in the SEMM expansion process. These models can differ significantly in terms of geometry and boundary conditions with respect to the real structure. Thus, a full analysis is performed to deduce how the accuracy of the numerical model in combination with the experimental model affects the consistency of the expansion process.

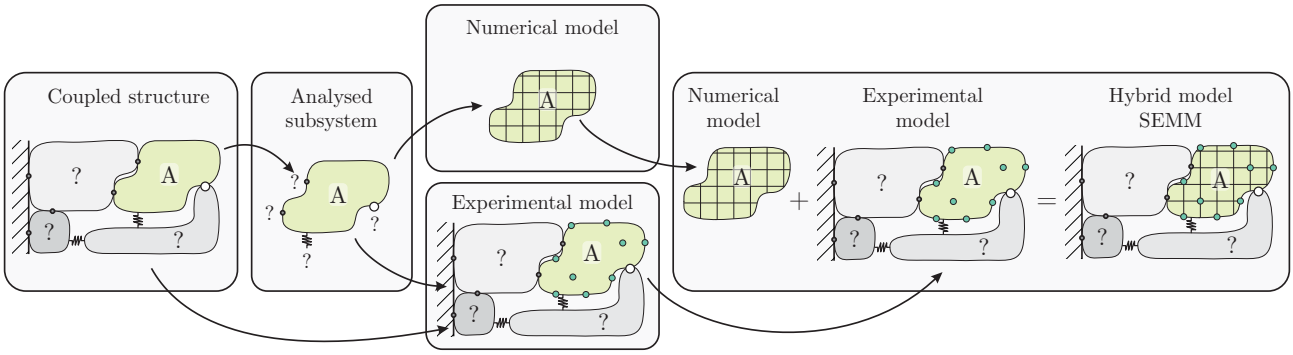

Figure 2: SEMM expansion process including quasi-equivalent models.

A fully extended form of the SEMM method (Eq. (8)) is applied as it is best suited for the expansion process. To combine quasi-equivalent models, the notation of the SEMM method is slightly adjusted:

$$\mathbf{Y}_{\text{in}}^{\text{SEMM}} = \mathbf{Y}_{\text{ex}}^{\text{par}} - \mathbf{Y}_{\text{ex}}^{\text{par}} \left(\begin{bmatrix} \mathbf{Y}_{\text{bi}} & \mathbf{Y}_{\text{bb}} \end{bmatrix}_{\text{ex}}^{\text{rem}} \right)^{+} \left(\begin{bmatrix} \mathbf{Y}_{\text{bb}} \end{bmatrix}_{\text{ex}}^{\text{rem}} - \mathbf{Y}_{\text{in}}^{\text{ov}} \right) \left(\begin{bmatrix} \mathbf{Y}_{\text{ib}} \\ \mathbf{Y}_{\text{bb}} \end{bmatrix}_{\text{ex}}^{\text{rem}} \right)^{+} \mathbf{Y}_{\text{ex}}^{\text{par}}, \tag{9}$$

where the index $\bullet_{\text{in}}$ refers to the included and index $\bullet_{\text{ex}}$ refers to the excluded. All the mixed models still describe the same structure; however, they can be considered as quasi-equivalent since they can differ in terms of geometry and applied boundary conditions. The overlay model is obtained experimentally by considering the component integrated into the entire system. The parent and removed models are based on a numerical model of the component, which is modelled independently of the overall system. Such an approach allows easier numerical modelling of a particular component. Since the numerical model of the analysed system does not include connections with other components, its dynamic properties do not correlate well with the actual situation.

4. Analysis of the method on an experimental case-study

The proposed SEMM-expansion method was used to expand the vibration response from a limited number of measured points on the side panel of a washing machine (Fig. 3). It represents a real complex structure whose accurate determination of the full-field response is essential to perform an effective vibro-acoustic optimization of the product. It is generally accepted that the design and especially the vibro-acoustic performance contribute to the customer perception of a premium product, and hence its value on the market.

Home appliances are designed in an increasingly modular fashion, combining in-house-developed products with outsourced components (Fig. 3a). With the increasing product complexity, the question arises as to how accurately, using only numerical models, the actual behaviour of the individual components (Fig. 3c) of the whole system can be represented. Alternatively, the vibration response of the structure could be measured at a limited number of points and then expanded to obtain a full-field vibration response.

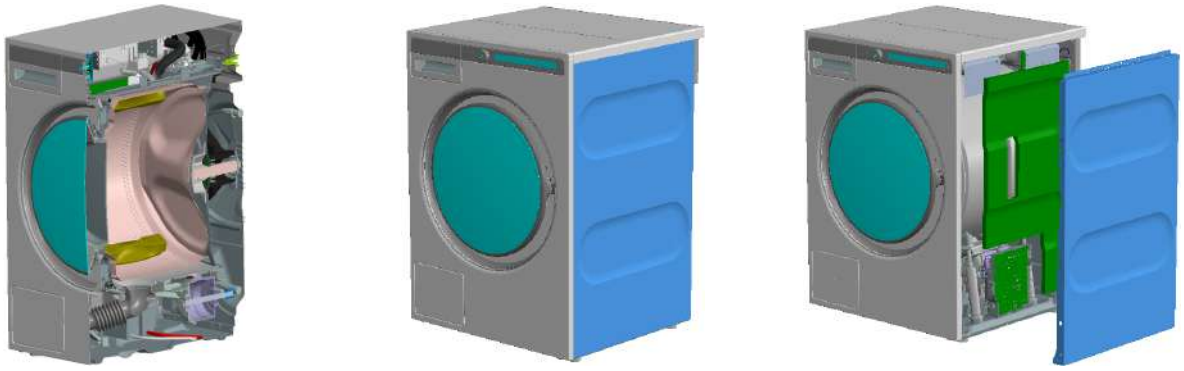

(a) (b) (c)

Figure 3: Analysed washing machine; a) cross-section, b) side panel included in the washing machine, c) exploded view of the analysed side panel.

This paper analyses the performance of the SEMM expansion process regarding the number and location of the excitation and response points in the experimental model, as well as with respect to the consistency of the numerical model. Therefore, five different numerical models were proposed in the expansion process, which differs in terms of geometry and boundary conditions. To assess the quality of the expansion process, FRAC [38] and MAC [39] criteria were used to compare the expanded full-field vibration response with the actual measured vibration response. The analysis aimed to check whether the modal shapes obtained and the FRFs are similar in shape to the reference ones, therefore these criteria, not accessing amplitudes, are sufficient. However, discrepancies in amplitudes can be observed using coherence criteria [2] or modal scale factor [39].

4.1. Experimental response model

The vibration response was experimentally obtained in the form of frequency-response functions (FRFs) with a side panel attached to the washing machine (Fig. 4a). To acquire the reference measurement, the structure was excited with a modal hammer (PCB 086C03 with a rubber tip) at 170 points, and seven triaxial accelerometers (PCB 356A32) were used to measure the response, as shown in Fig. 4b. To acquire signals, six signal acquisition modules with 24-bit resolution (NI 9234) were mounted to the measurement chassis (NI 9172). Signals were measured with a sampling rate of 25,6 kS/s with an acquisition time of one second.

Even though the system's response was measured only at seven points, it can be considered, from a mode shape point of view, as a high-resolution. Since the displacement receptance matrix is reciprocal, a high-resolution response can be obtained either by a large number of response points and a low number of excitation points [40] or vice versa, as was done in our case. By exploiting the reciprocity of the admittance matrix, the excitation at 170 points can be transposed and we can observe the response of the system at 170 response points. This high-resolution experimental model serves as a reference for assessing the quality of the expansion process.

Typically, the experimental model consists of a smaller number of excitation and response points. To analyse the performance of the SEMM expansion process, different combinations of measured DoFs are deduced from the entire experimental model. With this approach, it was possible to characterize the influence of the number and location of the excitation and response points on the accuracy of the expansion process.

The maximum rotational velocity of the washing machine is 2000 rpm (33 Hz), so the upper limit of the frequency range was set to 100 Hz. The modal testing was carried out with a soft rubber tip

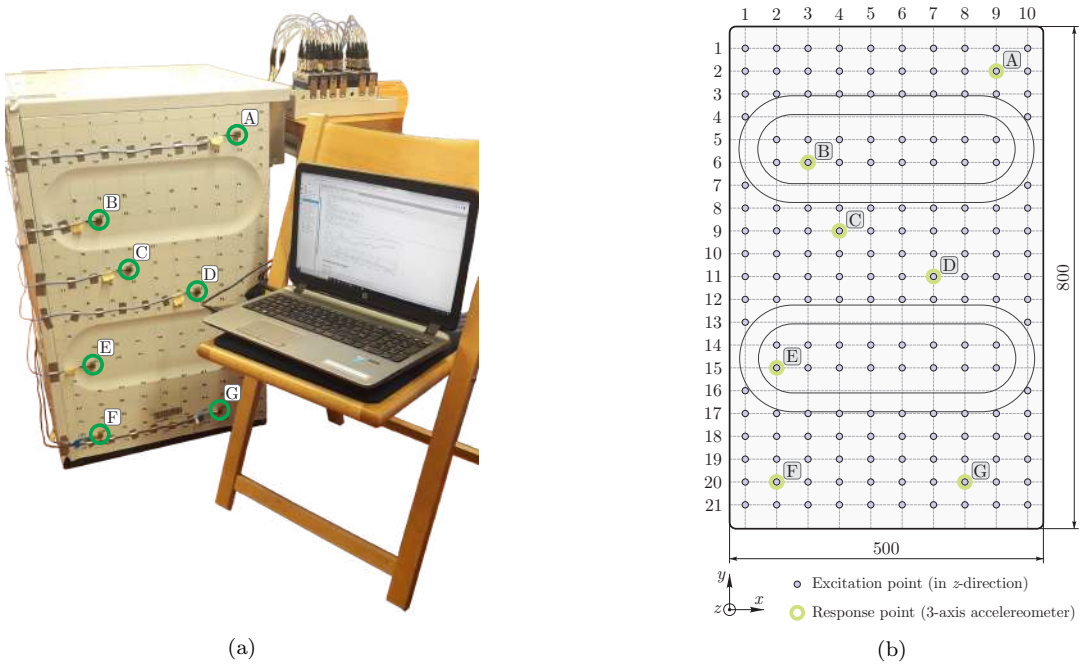

(a) (b)

Figure 4: Experimental modal analysis of side panel of washing machine; a) experimental setup, b) locations of response and excitation points.

on a modal hammer, which made it possible to excite the frequency range up to 100 Hz (Fig. 5). To consider frequencies above 100 Hz, the experiment must be performed with a harder hammer tip, which would shorten the pulses and thus excite a higher frequency range. In Fig. 6 all the measured FRFs in the z-direction are presented. It is possible to identify six natural frequencies (Table 1).

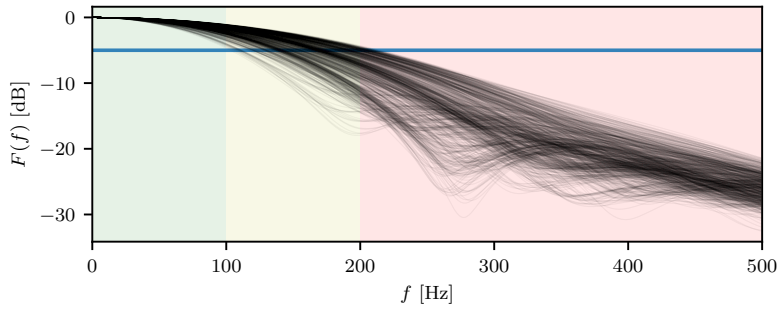

Figure 5: Force spectra using a soft tip on the modal hammer.

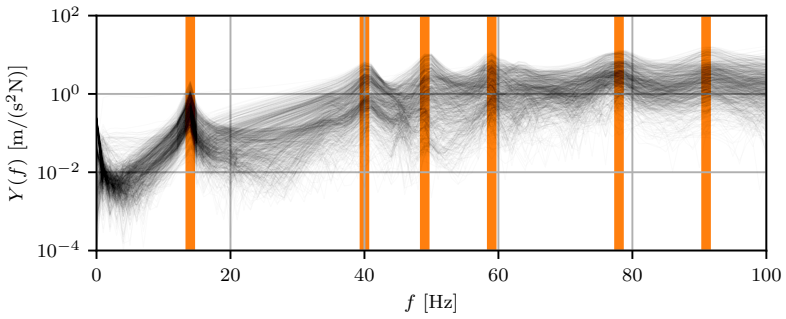

Figure 6: All experimentally obtained FRFs in z direction with marked identified natural frequencies.

The mode shapes (MS) of the analysed structure were obtained using the Complex Mode Indication Function (CMIF) [41]. Singular-value decomposition (SVD) is performed on the FRFs at each frequency

Table 1: Natural frequencies of side panel mounted to washing machine.

Natural freq.	1.	2.	3.	4.	5.	6.
Value [Hz]	14	40	49	59	78	91

point, resulting in a vector of singular values with the corresponding left and right singular vectors. The left singular vector represents the response modes, and the right singular vector represents the excitation modes. At the resonant frequencies, they can be considered as a good approximation of the mode shapes (Fig. 7) and the modal participation vectors, respectively. The first analysed mode represents the rigid displacement of the side panel due to the overall vibration response of the washing machine. All the other modes represent the distinct plate-like vibration modes of the side panel. The second and the third mode shapes are similar, and the reason for the 9 Hz difference between them is most likely due to the internal dynamics of the washing machine. The complex structure inside it results in two natural frequencies, close to each other, and are reflected in a very similar response of the plate.

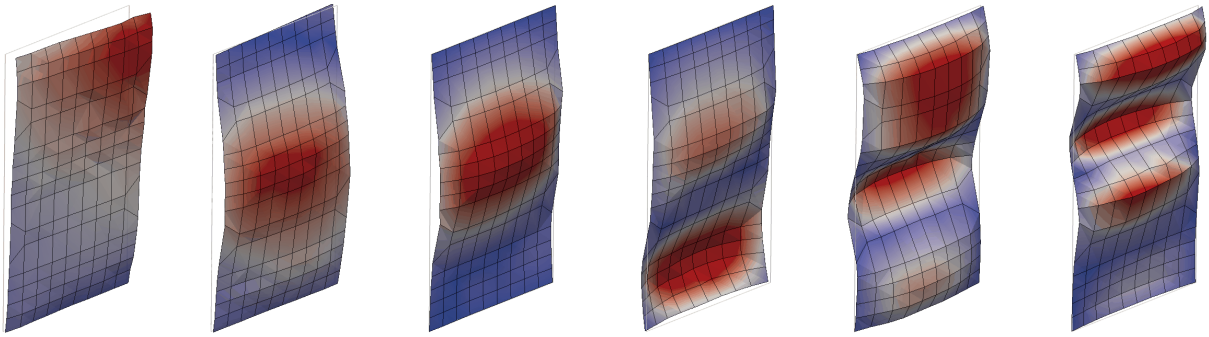

Figure 7: The first 6 experimentally acquired mode shapes of the analysed side panel mounted on the washing machine; a) 1st MS, b) 2nd MS, c) 3rd MS, d) 4th MS, e) 5th MS, f) 6th MS.

To prove the accuracy of the identified mode shapes using the CMIF method, the modal shapes were also determined with the multi-reference modal identification method [42]. Comparing both identified mode shapes with the MAC criterion (Fig. 8) a good correlation can be identified. The diagonal MAC values are not precisely of value one since were the compared mode shapes observed with different methods.

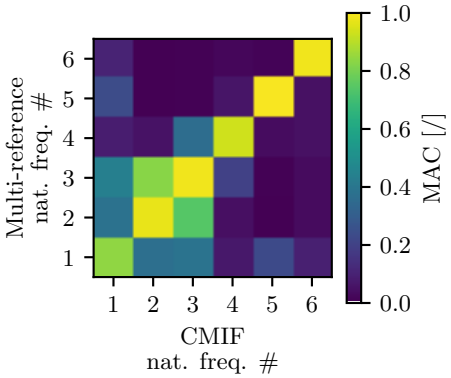

Figure 8: Comparison of experimental mode shapes with MAC criterion, provided by CMIF and multi-reference modal identification method.

4.2. Numerical model of analysed sub-component

The numerical model is constructed only for the side panel of the washing machine, as shown in Fig. 9a. The structure was modelled as a surface body (Fig. 9b) and meshed with 2D finite elements (Fig. 9c). Material properties are given in Table 2. With the numerical model was provided first 50 natural frequencies and corresponding mode shapes. FRFs were generated by the modal-superposition method, with damping neglect.

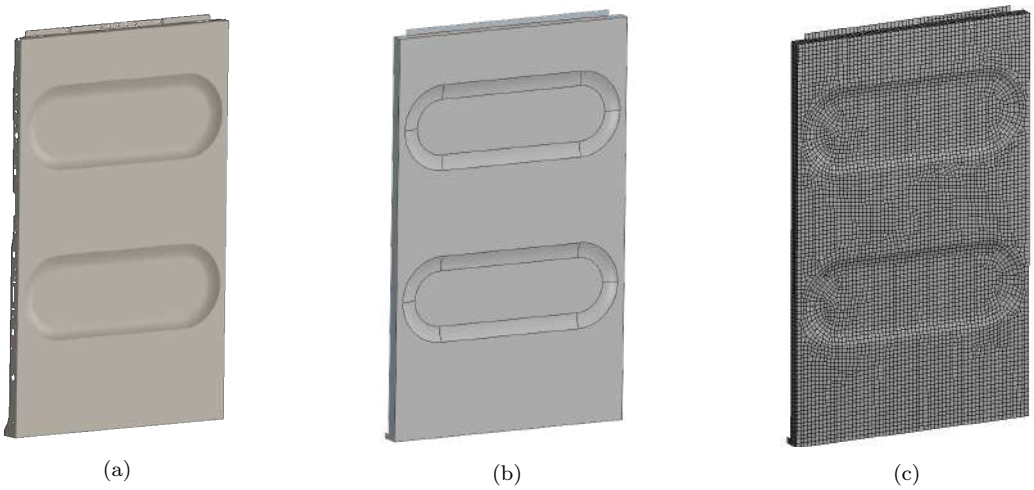

(a) (b) (c)

Figure 9: Development of numerical model for FEM analysis; a) original CAD model, b) simplified geometry, c) FEM model.

Table 2: Material properties of side panel.

Parameter	Thickness [mm]	Young's modulus [GPa]	Density [kg/m^3]	Poisson's ratio [/]
Value	0.8	200	7850	0.3

To identify the influence of the numerical model on the quality of the expansion process, five variations of the numerical model were analysed. The first three numerical models (Figs. 10a-10c) represent the exact geometry of the side panel and differ only concerning the applied boundary conditions. The fourth numerical model (Fig. 10d) represents the exact geometry of the side panel, but with the doubled thickness of the metal-sheet compared to the real structure. In the fifth numerical model (Fig. 10e) the geometry is considerably simplified compared to the actual geometry.

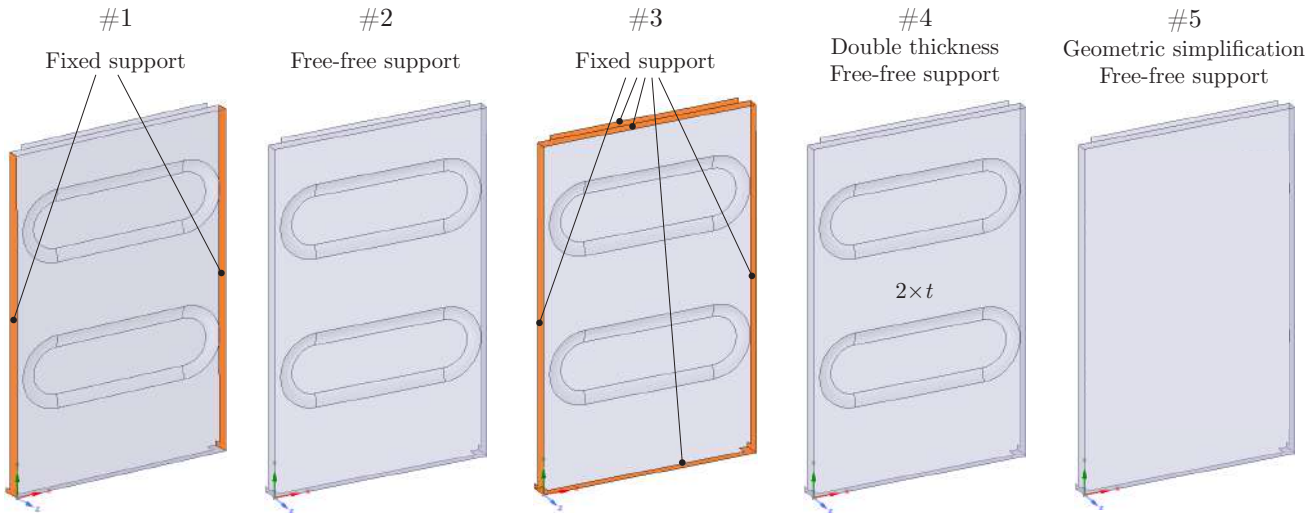

Figure 10: Numerical models; a) Model #1, b) Model #2, c) Model #3, d) Model #4, e) Model #5.

In Fig. 11 the FRFs are shown for all five numerical models that were obtained at driving point B (Fig. 4b) in the z-direction. In addition, the experimentally obtained FRF is also presented, which serves as a reference. From the comparison shown, it can be seen that by applying standard boundary conditions, none of the numerical models can accurately describe the real dynamic response of the side panel. In terms of the geometry and boundary conditions, the closest to the real state is model #1, which has fixed support on both long edges of the plate. This reflects the actual modelling difficulties since it is practically impossible to deduce valid boundary conditions when the given component is modelled independently of the whole system. Therefore, the entire expansion process will rely on the inclusion of a so-called quasi-equivalent numerical model, which may not even reflect the dynamic behaviour of a real structure.

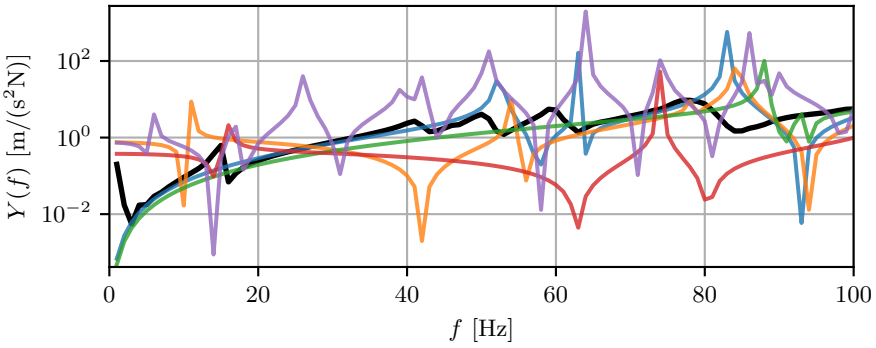

Figure 11: FRFs of different numerical model at driving point B.
(—) - Exp. model, (—) - Model #1, (—) - Model #2, (—) - Model #3, (—) - Model #4, (—) - Model #5

4.3. Sampling scheme and introduction of the aggregation index

To determine the influence of the experimental and numerical model parameters on the accuracy of the expansion, representative samples of possible parameter combinations were created. The sampling scheme considered the variation of the location and the number of excitation and response points in the experimental response model. The 25,000 possible parameter combinations were created using the Monte Carlo sampling scheme. The number of excitation points varied from 1 to 170 and the number of response points from 1 to 7. Their locations can only vary between given positions defined in the experimental setup presented in Fig. 4b.

The location of the excitation points is characterized by its distribution over the structure, using the methodology for animal and plant spatial populations [43]. The nearest-neighbour method was used to estimate the distribution of randomly selected excitation points. First, the mean distance to the nearest neighbour is calculated using the following equation:

$$\overline{r}_A = \frac{\sum_{i=1}^{n_e} r_i}{n_e}\,, \tag{10}$$

where r_i is the distance to the nearest neighbour for the individual location i and n_e is the number of all the excitation locations for the specific case. For the given analysed area with size A, the density of the excitation points is defined as:

$$\rho = \frac{n_e}{A} \tag{11}$$

and the expected distance to the nearest neighbour as:

$$\overline{r}_E = \frac{1}{2\sqrt{\rho}}\,. \tag{12}$$

A comparative parameter between the different excitation locations compares the actual average distance to the nearest neighbour with the expected distance. This parameter is called the aggregation index:

$$R = \frac{\overline{r}_A}{\overline{r}_E}\,. \tag{13}$$

If the spatial pattern is randomly generated in a given area, then the value of the parameter R is around 1. However, if the value of parameter R comes close to 0, this indicates clustering of the points at specific locations. In the case of spatially well-distributed points with minimal clustering, the parameter has values of around $R \approx 2$ or higher [43].

From Fig. 12 it can be seen that for a washing machine's side panel, a large distribution of points (large aggregation index) can only be achieved with a small number of excitation points. In the case of a large number of excitation points, their dispersion is limited, and the aggregation index can reach a maximum value of 1.8.

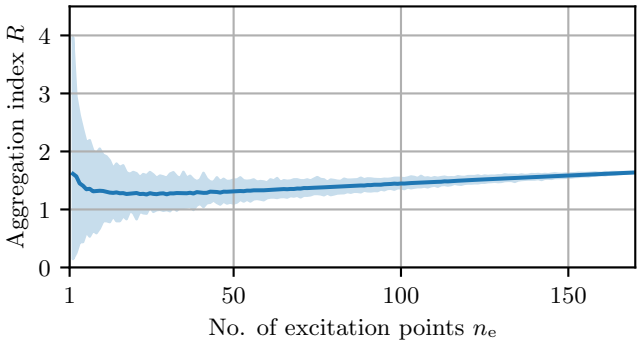

Figure 12: Max. and min. values of aggregation index for a given number of excitation points.

4.4. Parametric analysis

Once the sampling scheme is established it is possible to perform the expansion process and characterize its accuracy. The whole process is schematically presented in Fig. 13. During each iteration in the main loop the particular numerical model represented the parent model within the SEMM methodology. The overlay model is represented by an experimental response model that contains DoFs

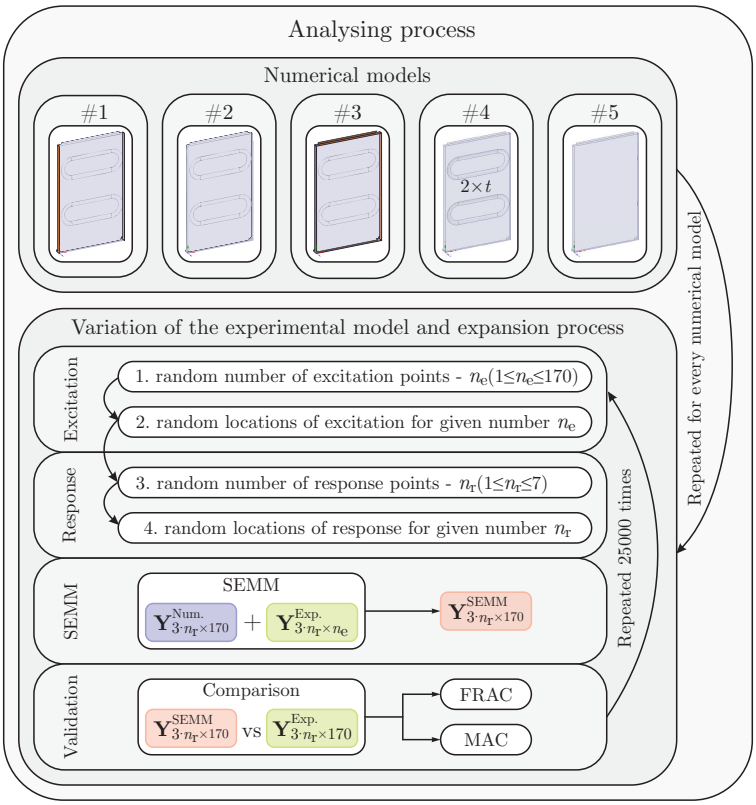

Figure 13: Parametric analysis.

according to a predefined sampling scheme. In the last step, the consistency of the expansion process is checked by comparing it with the experimental reference measurement using the FRAC and MAC criteria. All DoFs were included in the comparison process, both those contained in the experimental model (boundary DoFs) and extended ones (internal DoFs).

The results of the performed parametric analysis make it possible to characterize the influence of the system parameters on the quality of the expansion process. Fig. 14 shows the influence of the number of excitation points versus the aggregation index. The quality of the expansion process is assessed by comparing the expanded response with an experimentally obtained reference measurement using the FRAC and MAC criteria. A value of 1 indicates perfect agreement between compared measurements for both criteria.

Based on the presentation in Fig. 14 it is clear that the accuracy of the expanded displacement field improves when increasing the number of excitation points and the number of response points. It is evident that the numbers of response and excitation points have the greatest influence on the quality of the expansion process. However, to clearly demonstrate the influence of each individual parameter, a more detailed analysis is performed.

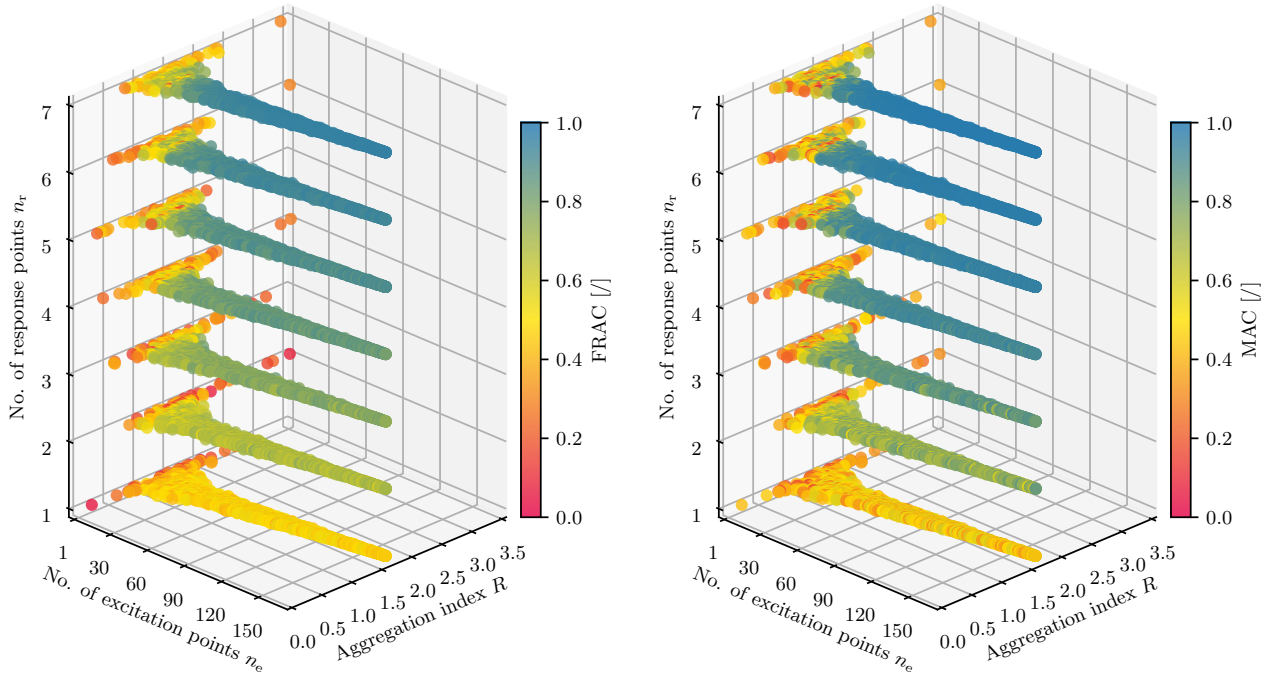

Figure 14: Results of parametric analysis with numerical model #1;
a) FRAC criterion, b) MAC criterion.

4.4.1. Influence of the aggregation index and the number of excitation points

The aggregation index was used to analyse the influence of the excitation points' distribution over the analysed object with regard to the quality of the expansion process. The physical significance of the aggregation index is shown in Fig. 15, where three characteristic values of this parameter are shown. The data present different configurations taken from the whole set of 25,000 possible combinations. Based on the presented excitation-point distribution, it is evident that higher aggregation values indicate a more even distribution of points over the whole geometry of the structure.

The influence of the aggregation index on the quality of the expansion process is shown in Fig. 16 by evaluating the MAC and FRAC criteria. It is clear that the aggregation index is strongly correlated with the number of excitation points in the system. As the number of excitation points increases, their scattering over the entire considered surface also increases. Their locations are not arbitrary and can be located only at previously defined locations of the experimental model (Fig. 4b).

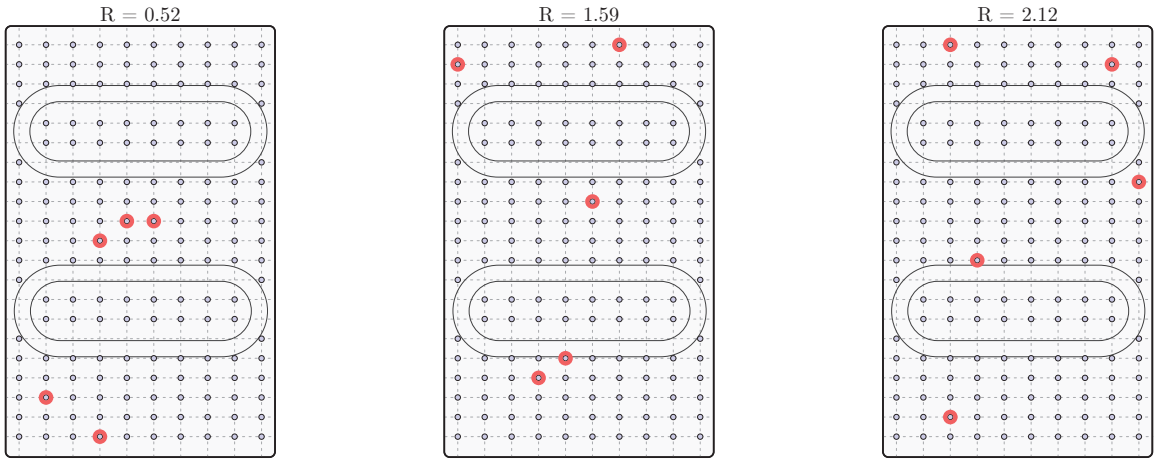

(a) (b) (c)

Figure 15: Examples of different distributions of excitation points; a) lightly clustered distribution, b) random distribution, c) regular distribution.

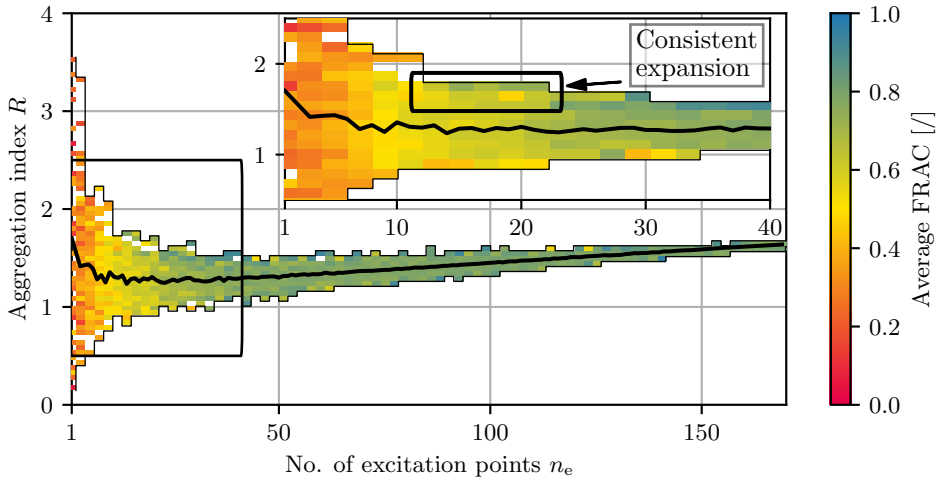

(a)

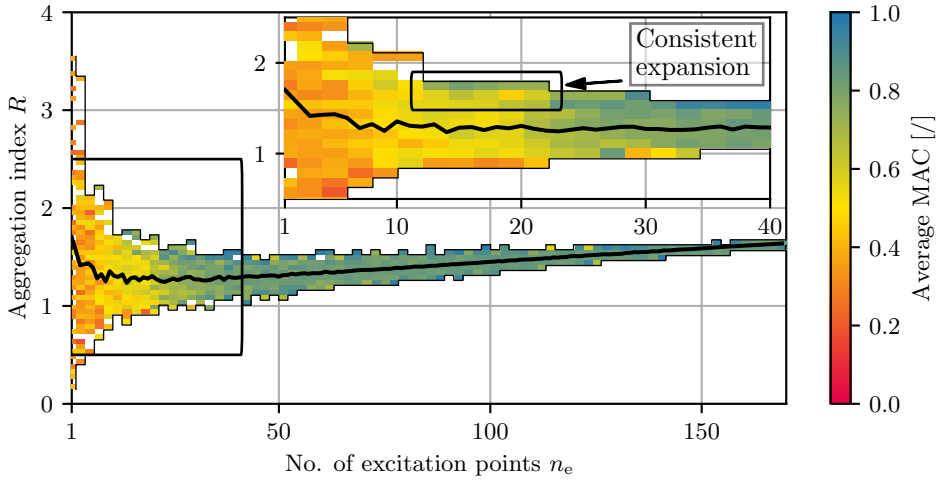

(b)

Figure 16: Relation between the aggregation index R and the average FRAC and MAC values regarding the number of excitation points in the experimental model in the case of the numerical model #1; a) FRAC, b) MAC.
( ) - no data

As seen in Fig. 14, the increase in the accuracy of the expansion process is greatly influenced not only by increasing the number of response points but also by increasing the number of excitation points, which is particularly evident in Fig. 16. By increasing the number of excitation points, it is possible to perform a consistent expansion process, which can be indicated by the high values of the MAC and FRAC criteria. This is fairly obvious, yet the goal of any expansion process is to deduce a full-field vibration response with as few as possible measured (excitation) points. Identifying the configurations with a relatively small number of excitation points and a high aggregation index can also result in a well-defined expansion process. Therefore, the charts in Fig. 16 are of great importance, as it is possible to identify the parameter configurations that enable an accurate expansion process with a relatively small number of excitation points. This region is zoomed-in in Fig. 16, where the area of consistent expansion with a low number of excitation points is also marked.

Using the same analysis procedure could be determined the optimal sensor placement. In the presented case, such analysis would not be relevant since only seven response sensors were available. However, if the experimental model consists of a higher number of response points, it makes sense to identify the locations of the response points that give the best expansion results.

4.4.2. Influence of the number of the response and excitation points

It has been shown that the number of excitation points has an important influence on the consistency of the expansion process. In Fig. 17 the average FRAC and MAC values for the expanded and reference configurations are shown versus the number of excitation and response points. The intense lines represent the average value of a single criterion for a given number of response points. The corresponding shaded regions represent the area of standard deviation where there are 68.27 % of all the results. When performing the experiment, a maximum of seven three-axis accelerometers (response points) were used, which were located randomly across the side panel of the washing machine (Fig. 4).

From Fig. 17 it is clear that for a small number of excitation points (between 1 and 30), an additional

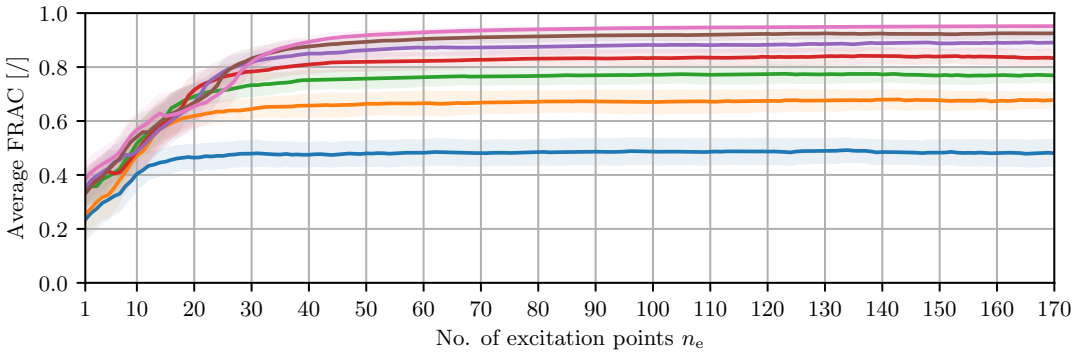

(a)

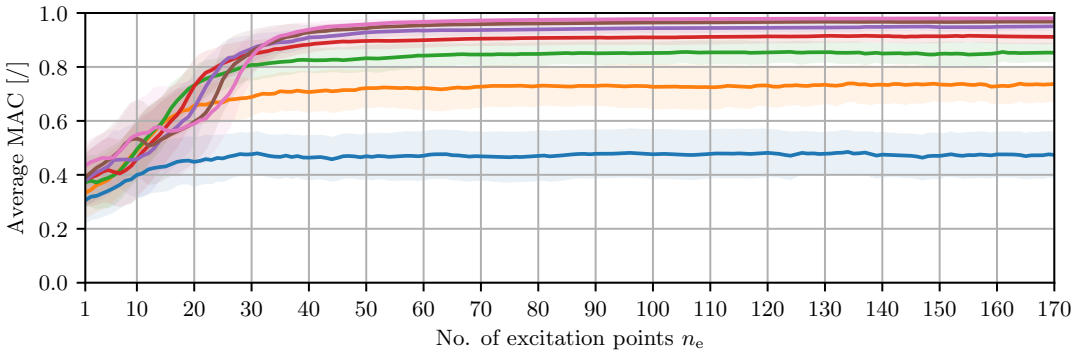

(b)

Figure 17: Influence of number of response and excitation points in experimental modal in the case of the numerical model #1; a) FRAC criterion, b) MAC criterion.
No. of acc.: (—) - 1, (—) - 2, (—) - 3, (—) - 4, (—) - 5, (—) - 6, (—) - 7

excitation point can contribute significantly to the accuracy of the expansion process. A small number of excitation points can lead to an inconsistent reconstruction of the vibration response, since the experimental model lacks information regarding the dynamic properties of the analysed structure. In addition, a higher aggregation index (Figure 16) implies a better dispersion of the points, which leads to a greater accuracy of the expansion process.

It is obvious that the greater the number of response and excitation points, the better the accuracy of the expansion process. When at least 40 excitation points are included in the formulation, each additional point only slightly improves the accuracy of the expansion. In this region, every additional response point considerably improves the expansion accuracy, while the number of excitation points has a negligible effect on expansions accuracy. In this case, an exponent dependency on the values of the FRAC and MAC criteria can be observed with regard to the number of response points. Based on the presented analysis, it can be concluded that 40 excitation points together with measurements at four response points would guarantee a consistent expansion process for the given application.

4.4.3. Influence of the numerical model

This section presents the influence of the numerical model on the consistency of the expansion process. Five different numerical models are considered within the expansion process, as shown in Fig. 10. In general, it is clear (Fig. 18) that the most accurate expansion process can be obtained with numerical models #1 and #2. It is somehow expected that #1 numerical model will perform well since the boundary conditions are the most similar to the actual fixation of the side panel in the washing machine (Fig. 4a). On the other hand, the good performance of the numerical model #2 is surprising. Since free-free boundary conditions are proposed, the dynamics of the numerical model do not reflect the actual behaviour of a given system. However, good performance can derive from the fact that in this case the interconnections between the DoFs are still defined in a consistent manner. It is evident that in the case of a freely supported structure, the influence of the boundary conditions can be efficiently "updated" by the integration of the experimental response model and that presents

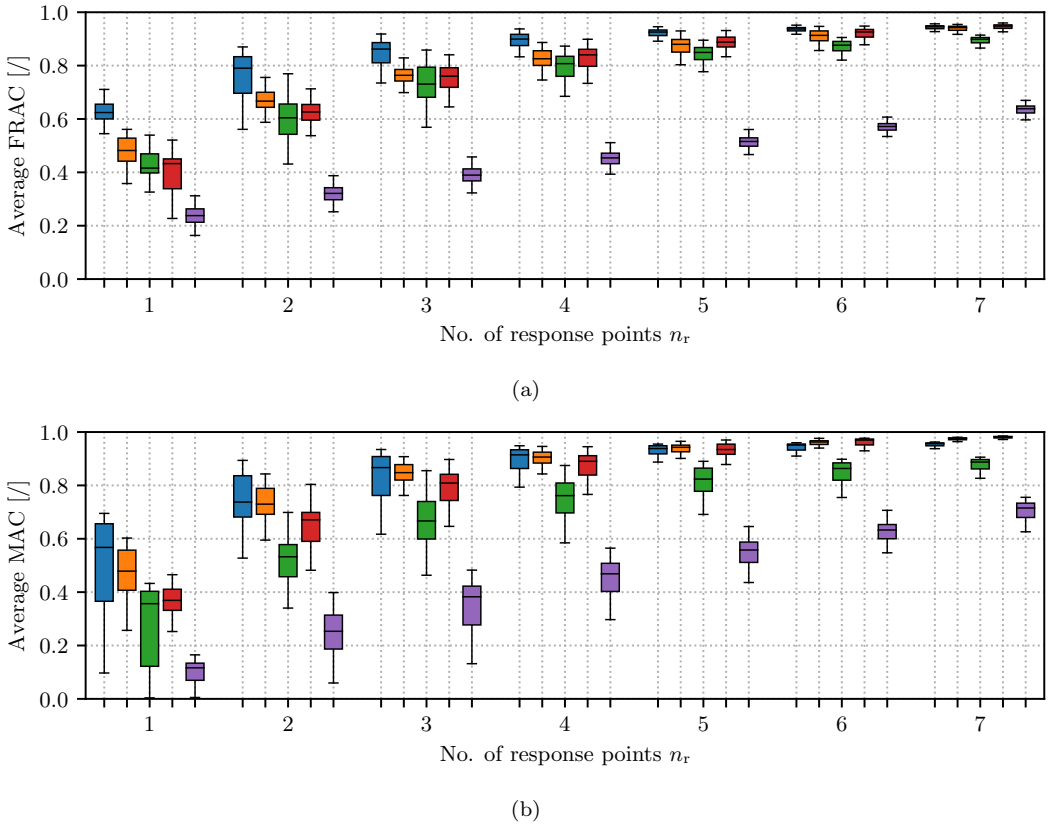

Figure 18: Influence of number of response points and different numerical models; a) FRAC criterion, b) MAC criterion. Numerical model: (■) - #1, (■) - #2, (■) - #3, (■) - #4, (■) - #5

the main advantage of the proposed method.

In addition, Fig. 18 clearly demonstrates that only measurements at multiple response points guarantee an accurate expansion process. The values of FRAC and MAC criterion above 0.9 are usually considered as good matching between compared results. In the presented case, five response points are sufficient to meet that condition for an accurate expansion process if the numerical model #1 or #2 was to be considered.

The expansion process using the numerical model #3 results in lower values of the MAC and FRAC criteria. This is somehow expected as the numerical model #3 proposes fixed boundary conditions at all four edges, which does not reflect the actual fixation of the side panel to the washing machine's structure. Due to the applied boundary conditions, the physical interconnection between edge DoFs no longer represents a consistent basis for expanding the experimental model. In the case of the numerical model #4, a slightly lower accuracy of the expansion process is observed due to an incorrectly defined thickness. This is due to the fact that the consistency of the physical connection between the DoFs over the entire structure of the side panel is not correctly defined.

In an expansion process with the numerical model #5, over-simplifying the geometry significantly affects the consistency of the interconnections between the DoFs. Because of the incorrectly defined geometry, the relationship between the DoFs is not correctly defined, so this numerical model cannot be considered as a consistent basis for the expansion process.

4.4.4. Demonstration of the expansion process using the SEMM method

The results of the presented analysis can be summarized in a comprehensive diagram (Fig. 19), representing the influence of all the analysed parameters. This diagram shows the average values of

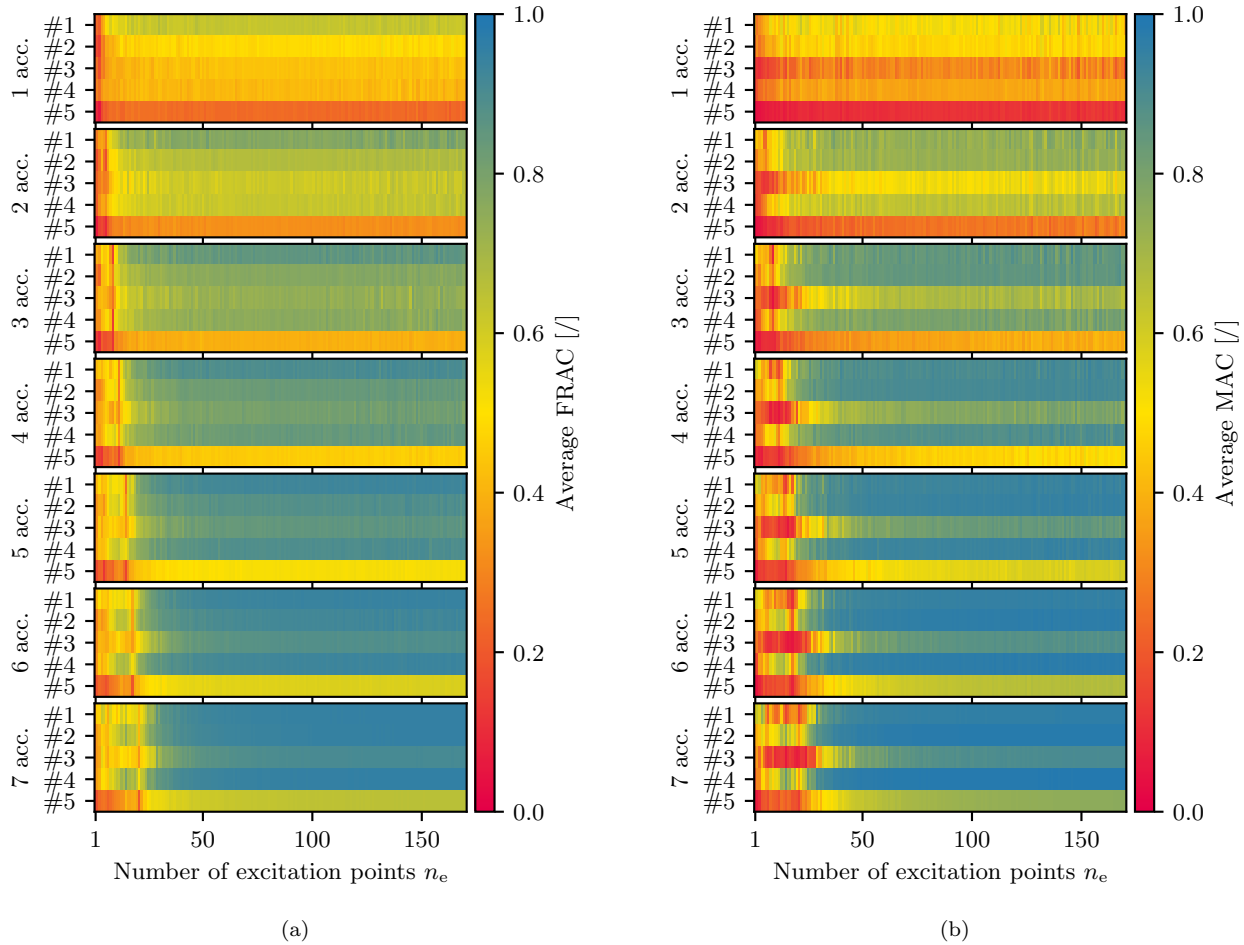

Figure 19: Accuracy of expansions process versus the number of response and excitation points considering different numerical models; a) FRAC criterion, b) MAC criterion.

the MAC and FRAC criteria versus the numerical model and the number of excitation and response points in the experimental response model. Based on this representation, it is evident that minimum requirements to obtain a satisfactory expansion process in to include at least three response points in the experimental response model. In addition, the SEMM expansion process should be performed with either numerical model #1 or #2.

Here, the example of the expansion process is presented with numerical model #1 in conjunction with an experimental model having three response points and 15 excitation points, as shown in Fig. 21b. The configuration with the highest aggregation index is selected from all the possible configurations with these parameters. As shown in Fig. 20 a high value of the aggregation index closely correlates with the accuracy of the expansion process. For the selected configuration, the aggregation index has a value of $R = 1.75$, which indicates well-distributed excitation points all over the analysed structure.

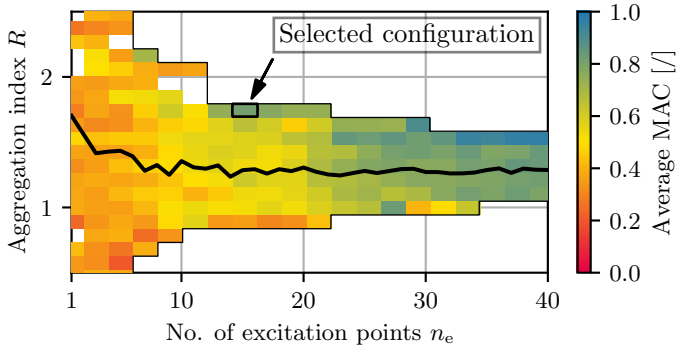

Figure 20: Accuracy of the expansion process versus aggregation index R and number of excitation points considering numerical model #1.

The entire expansion process was performed using the pyFBS package [40], as shown in Fig. 21a. pyFBS is an open-source package written in Python and also includes the SEMM method. A mesh of the structure was generated using Ansys 2019 R3, where the mass and stiffness matrices were also defined. Using the pyFBS package, FRFs were generated in all the DoFs considered in the numerical model using the model superposition method with the first 50 modes. Hence, the numerical model consists of 170 excitation points in a single direction and three response points in all three directions. The schematic presentation of the experimental response model's receptance matrix is shown in Fig. 22,

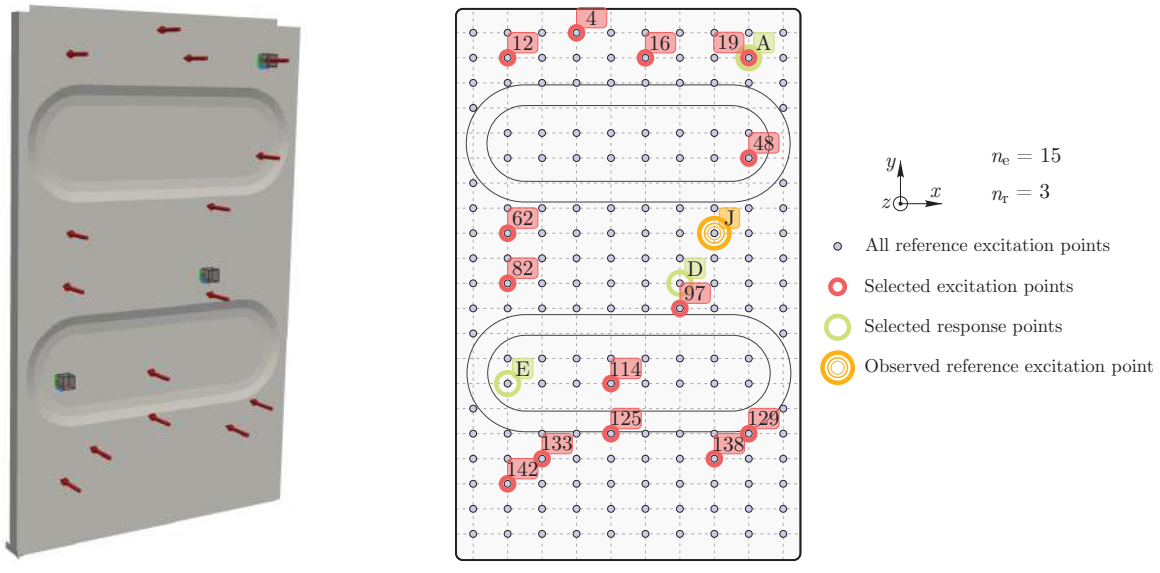

(a) (b)

Figure 21: Schematic depiction of selected points contained in experimental model; a) experimental model in pyFBS package, b) detailed presentation of observed points.

together with the numerical receptance matrix.

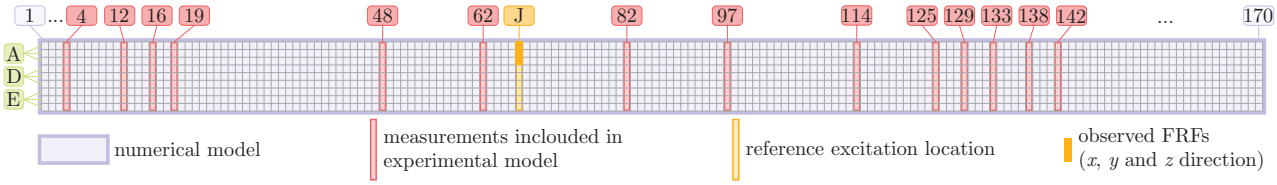

Figure 22: Schematic presentation of receptance matrix of numerical and experimental model for expansion process.

After the expansion process, it was possible to establish the hybrid model and deduce the corresponding model parameters. The values of the natural frequencies and damping ratios are presented in Table 3. It is evident that the proposed expansion process inherits the real-life dynamic properties from the experimental model. It is clear that the natural frequencies and damping ratios of the hybrid model are practically identical to the experimentally obtained values. The corresponding mode shapes were determined using the CMIF method (Fig. 23). Based on the visual comparison and evaluation of the MAC criterion (Fig. 24) good agreement with an experimental reference can be confirmed. In addition, the comparisons of the FRFs in all three response directions between points A and J are shown in Fig. 25. The experimental reference and the expanded solution are presented along with numerically obtained FRFs. Based on this comparison, good performance of the expansion process can be observed.

Table 3: Comparison of modal parameters between reference experimental model and SEMM-expanded model.

Natural freq. #		1.	2.	3.	4.	5.	6.
Freq. [Hz]	Exp.	13,8	40,6	49,3	58,8	78,1	91,3
	SEMM	13,8	40,5	49,3	58,7	74,4	91,4
Damp. [%]	Exp.	1,96	2,64	1,61	1,88	3,54	2,32
	SEMM	1,88	2,74	2,21	1,64	4,06	2,92

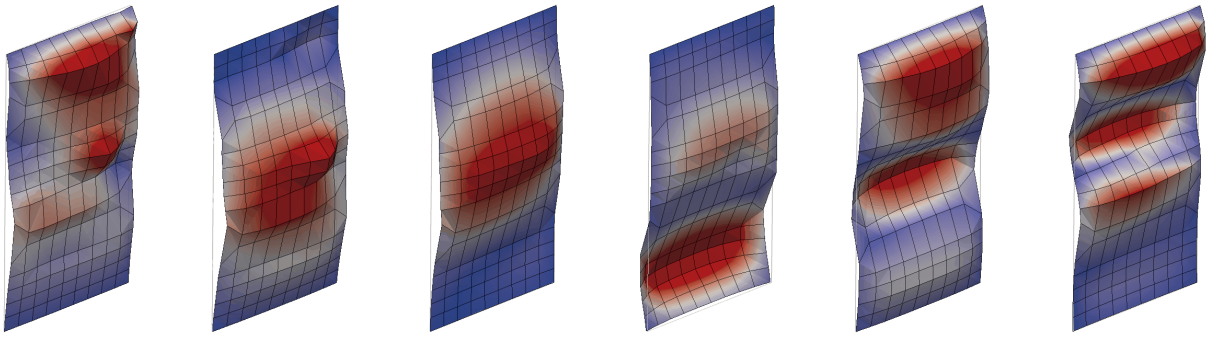

(a) (b) (c) (d) (e) (f)

Figure 23: Reconstructed first 6 mode shapes of analysed side panel mounted on washing machine; a) 1st MS, b) 2nd MS, c) 3rd MS, d) 4th MS, e) 5th MS, f) 6th MS.

The expansion process enables the measurement to be expanded to unmeasured points, and in addition, it "updates" the dynamic properties of the numerical model based on the inclusion of an experimental response model. Given that the expansion process was carried out with a relatively small number of response and excitation points, it still proves to be highly efficient if the expansion parameters are properly selected.

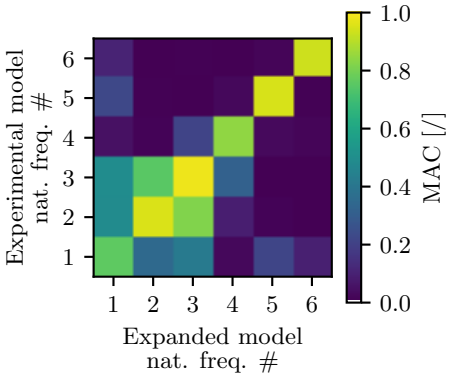

Figure 24: MAC criterion between reconstructed and reference experimental model.

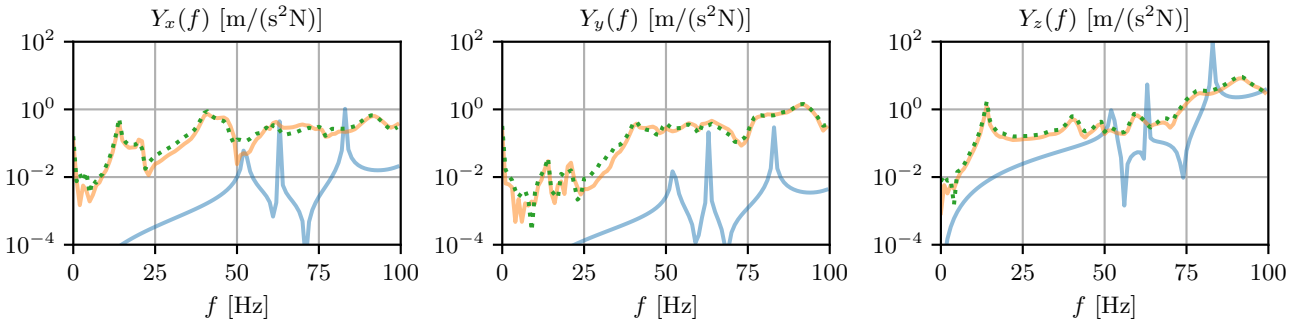

Figure 25: FRF comparison between response at point A (all three directions) and excitation at point J (in z-direction); a) resp. in x direction, b) resp. in y direction, c) resp. in z direction.
— - num., — - exp., ····· - SEMM expansion.

5. Conclusion

This study provides a comprehensive analysis of the parameters influencing the quality of the SEMM expansion process. Traditionally, the SEMM method is used to couple the experimental and numerical models of the same system. In this article, the expansion process from the limited measurement to full-field dynamic response is performed using a so-called quasi-equivalent numerical model. As shown in the presented case study, it is challenging to develop a valid numerical model of the sub-component while embedded in the system, especially due to the complex connectivity conditions at the interface with other sub-components.

The SEMM expansion process is more accurate the more excitations and response points are included in the experimental response model, which is an obvious finding. Systematic parametric analyses have proved that it is possible to get an accurate expansion process with a relatively small number of response and excitation points. This is feasible only when the experimentally observed DoFs are well scattered over the given object, and the numerical model presents a consistent description of the connectivity between the DoFs. High values of the aggregation index directly imply a higher dispersion of DoFs included in the experimental model, which results in a more accurate expansion process, especially with a small number of excitation points. The SEMM expansion method works best if the experimental model contains impact and response DoFs, distributed over the analysed structure. Good observability and controllability of the system is crucial step for accurate expansion results. The number and location of impact and response points are therefore case-specific.

A successful expansion is also closely correlated with the consistency of the numerical model. In the presented case this was mainly influenced by the geometry of the component, while the mass and stiffness properties turn out to be less influential. While it is hard to quantify the generality of this conclusion based on one single result, it must be noted that the changes made to mass and stiffness

where significant and the changes in the geometry's simplicity were within reason. Therefore, the authors find this conclusion to be generally applicable to similar components.

The final experimental demonstration showed that the SEMM-expansion process can serve as an efficient and accurate method for evaluating the full-field dynamic response of real complex systems through proper parameter selection. To use the proposed methodology for different applications, it is necessary to establish a reference model. Using the presented systematic analysis the sufficient number and locations of excitation and response points is determined together with the appropriate numerical model. In the following iterations of product development, a full-field dynamic response can be predicted using a limited number of measured points, which reduces the time required for the examination of the individual development stage.

Acknowledgements

The authors acknowledge the partial financial support from the core research funding P2-0263 and applied research project L2-1837, both financed by ARRS, Slovenian research agency.

References

[1] D. De Klerk, Dynamic response characterization of complex systems through operational identification and dynamic substructuring-an application to gear noise propagation in the automotive industry, Ph.D. thesis, Delft University of Technology (2009).

[2] M. V. van der Seijs, Experimental dynamic substructuring: Analysis and design strategies for vehicle development, Ph.D. thesis, Delft University of Technology (2016).

[3] D. A. Ehrhardt, M. S. Allen, S. Yang, T. J. Beberniss, Full-field linear and nonlinear measurements using continuous-scan laser doppler vibrometry and high speed three-dimensional digital image correlation, Mechanical Systems and Signal Processing 86 (2017) 82–97.

[4] F. Trainotti, T. F. Berninger, D. J. Rixen, Using laser vibrometry for precise FRF measurements in experimental substructuring, in: Dynamic Substructures, Volume 4, Springer, 2020, pp. 1–11.

[5] H. Khalil, D. Kim, J. Nam, K. Park, Accuracy and noise analyses of 3d vibration measurements using laser doppler vibrometer, Measurement 94 (2016) 883–892.

[6] M. N. Helfrick, C. Niezrecki, P. Avitabile, T. Schmidt, 3d digital image correlation methods for full-field vibration measurement, Mechanical systems and signal processing 25 (3) (2011) 917–927.

[7] F. Trebuňa, M. Hagara, Experimental modal analysis performed by high-speed digital image correlation system, Measurement 50 (2014) 78–85.

[8] Y. Chen, P. Logan, P. Avitabile, J. Dodson, Non-model based expansion from limited points to an augmented set of points using Chebyshev polynomials, Experimental Techniques 43 (5) (2019) 521–543.

[9] E. Dascotte, Model updating for structural dynamics: past, present and future outlook, in: International Conference on Engineering Dynamics (ICED), Carvoeiro, Algarve, Portugal, 2007, pp. 16–18.

[10] M. S. Mohd Zin, M. N. Abdul Rani, M. A. Yunus, W. I. I. Wan Iskandar Mirza, A. Azlan, Z. Mohamed, Modal and frf based updating methods for the investigation of the dynamic behaviour of a plate, Journal of Mechanical Engineering (2017) 175–189.

[11] M. Friswell, J. E. Mottershead, Finite element model updating in structural dynamics, Vol. 38, Springer Science & Business Media, 2013.

[12] Y. Chen, A non-model based expansion methodology for dynamic characterization, Ph.D. thesis, University of Massachusetts Lowell (2019).

[13] Y. Chen, P. Avitabile, C. Page, J. Dodson, A polynomial based dynamic expansion and data consistency assessment and modification for cylindrical shell structures, Mechanical Systems and Signal Processing 154 (2021) 107574.

[14] E. Balmès, Review and evaluation of shape expansion methods, in: International Modal Analysis Conference, 2000, pp. 555–561.

[15] J. O'Callahan, P. Avitabile, R. Riemer, System equivalent reduction expansion process (SEREP), in: Proceedings of the 7th international modal analysis conference, Vol. 1, Union College Schnectady, 1989, pp. 29–37.

[16] Y. Chen, D. Joffre, P. Avitabile, Underwater dynamic response at limited points expanded to full-field strain response, Journal of Vibration and Acoustics 140 (2018) 051016.

[17] K. Bharadwaj, A. Sheidaei, A. Afshar, J. Baqersad, Full-field strain prediction using mode shapes measured with digital image correlation, Measurement 139 (2019) 326–333.

[18] Y. Chen, P. Avitabile, J. Dodson, Data consistency assessment function (DCAF), Mechanical Systems and Signal Processing 141 (2020) 106688.

[19] L. Thibault, A. Butland, P. Avitabile, Variability improvement of key inaccurate node groups–VIKING, in: Topics in Modal Analysis II, Volume 6, Springer, 2012, pp. 603–624.

[20] S. W. Klaassen, M. V. van der Seijs, D. de Klerk, System equivalent model mixing, Mechanical Systems and Signal Processing 105 (2018) 90–112.

[21] D. de Klerk, D. J. Rixen, J. de Jong, The frequency based substructuring (FBS) method reformulated according to the dual domain decomposition method, in: Proceedings of the 24th International Modal Analysis Conference, A Conference on Structural Dynamics, 2006, pp. 1–14.

[22] N. Maia, J. Silva, Modal analysis identification techniques, Philosophical Transactions of the Royal Society of London. Series A: Mathematical, Physical and Engineering Sciences 359 (1778) (2001) 29–40.

[23] C.-X. Qu, T.-H. Yi, H.-N. Li, B. Chen, Closely spaced modes identification through modified frequency domain decomposition, Measurement 128 (2018) 388–392.

[24] Y. Yang, S. Nagarajaiah, Output-only modal identification with limited sensors using sparse component analysis, Journal of Sound and Vibration 332 (19) (2013) 4741–4765.

[25] M. Pogačar, T. Bregar, G. Čepon, M. Boltežar, Near-to-node modal identification using multiple related response models, Measurement 171 (2021) 108793.

[26] Z. Saeed, S. W. Klaassen, C. M. Firrone, T. M. Berruti, D. J. Rixen, Experimental joint identification using system equivalent model mixing in a bladed disk, Journal of Vibration and Acoustics 142 (5) (2020).

[27] T. Bregar, K. Zaletelj, G. Čepon, J. Slavič, M. Boltežar, Full-field FRF estimation from noisy high-speed-camera data using a dynamic substructuring approach, Mechanical Systems and Signal Processing 150 (2021) 107263.

[28] M. Kodrič, G. Čepon, M. Boltežar, Experimental framework for identifying inconsistent measurements in frequency-based substructuring, Mechanical Systems and Signal Processing 154 (2021) 107562.

[29] Z. Saeed, C. M. Firrone, T. M. Berruti, Hybrid Numerical-Experimental Model Update Based on Correlation Approach for Turbine Components, Journal of Engineering for Gas Turbines and Power 143 (4) (02 2021).

[30] D. Ocepek, M. Kodrič, G. Čepon, M. Boltežar, On the estimation of structural admittances from acoustic measurement using a dynamic substructuring approach, Applied Acoustics 180 (2021) 108115.

[31] E. Pasma, S. Klaassen, L. Nieuwenhuijse, M. van der Seijs, D. Lennström, Application of system equivalent model mixing (SEMM) to model the structural dynamic properties of a complex vehicle component using numerical and experimental data, in: Proceedings of ISMA2018 and USD2018. International Conference on Noise and Vibration Engineering, 2018, pp. 4037–4047.

[32] S. Klaassen, M. van der Seijs, Introducing semm: A novel method for hybrid modelling, in: Dynamics of Coupled Structures, Volume 4, Springer, 2018, pp. 117–125.

[33] D. de Klerk, D. J. Rixen, S. Voormeeren, General framework for dynamic substructuring: history, review and classification of techniques, AIAA journal 46 (5) (2008) 1169–1181.

[34] S. Klaassen, M. V. van der Seijs, Introducing SEMM: A novel method for hybrid modelling, in: Dynamics of Coupled Structures, Volume 4. Conference Proceedings of the Society for Experimental Mechanics Series, Springer International Publishing, 2018, pp. 117–125.

[35] A. Linderholt, T. Abrahamsson, A. Johansson, D. Steinepreis, P. Reuss, A comparison of the dynamic behavior of three sets of the ampair 600 wind turbine, in: M. Allen, R. L. Mayes, D. J. Rixen (Eds.), Dynamics of Coupled Structures, Volume 4, Springer International Publishing, Cham, 2015, pp. 99–110.

[36] W. W. I. Mirza, M. A. Rani, M. Yunus, R. Febrina, M. Sani, Estimating rotational FRFs of a complex structure using FE model updating, mode expansion and FRF synthesis method, IOP Conference Series: Materials Science and Engineering 807 (2020) 012045.

[37] S. W. B. Klaassen, D. J. Rixen, The inclusion of a singular-value based filter in SEMM, in: Proceedings of the 38th International Modal Analysis Conference, A Conference on Structural Dynamics, 2020.

[38] W. Heylen, S. Lammens, FRAC: a consistent way of comparing frequency response functions, in: International Conference on Identification in Engineering, 1996, pp. 48–57.

[39] R. J. Allemang, D. L. Brown, A correlation coefficient for modal vector analysis, in: Proceedings of the 1st International Modal Analysis Conference, Vol. 1, 1982, pp. 110–116.

[40] Y. Chen, A. S. E. Mendoza, D. T. Griffith, Experimental and numerial study of high-order complex curvature mode shape and mode coupling on a three-bladed wind turbine assembly, Mechanical Systems and Signal Processing 160 (2021) 107873.

[41] C. Shih, Y. Tsuei, R. Allemang, D. Brown, Complex mode indication function and its applications to spatial domain parameter estimation, Mechanical systems and signal processing 2 (4) (1988) 367–377.

[42] B. Peeters, M. El-kafafy, P. Guillaume, The new PolyMAX Plus method: confident modal parameter estimation even in very noisy cases, in: Proceedings of the ISMA, 2012, pp. 2801–2813.

[43] C. J. Krebs, Ecological Methodology, The Benjamin/Cummings series in the life sciences, Benjamin/Cummings, 1999.